METHODOLOGY STUDY OF GEOTHERMAL RESOURCE EVALUATION USING REMOTE-SENSING AND GROUND-SURFACE TEMPERATURE DATA, BURWASH LANDING, YUKON – STATUS AND PRELIMINARY RESULTS

Z. Chen[1], S.E. Grasby[1], W. Yuan[1], M. Colpron[2], and X. Liu[1]

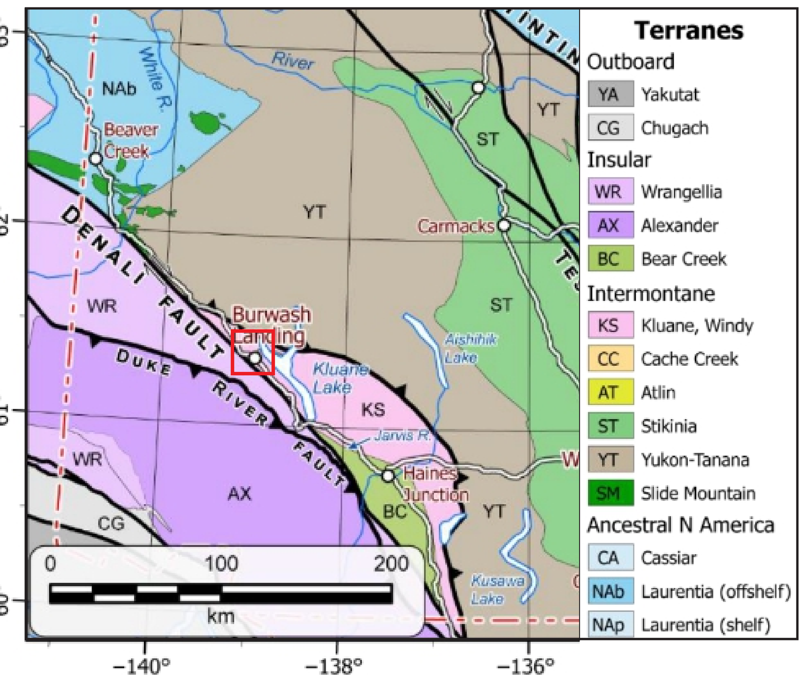

Figure 1. A geological map showing regional geological setting and location of the study area. The study area of the Burwash Landing is within the Denali fault zone (Map modified from © 2023, Government of Yukon)

Ground Surface Temperature Method

The GST method is based on conservation principle that the rate of ground heat energy change in time is equal to the heat flux through boundary, which can be expressed by the following heat equation:

$$\rho C_p \frac{\partial T}{\partial t} = \lambda \frac{\partial^2 T}{\partial x^2} \tag{1}$$

where T is the temperature (°C), t is time (s), λ: thermal conductivity (W m^{-1}K^{-1}), ρ: density (kg/m^3), C_p thermal capacity (J kg^{-1} K^{-1}) and x burial depth (m) below ground surface. Solving the equation with initial and boundary conditions, Eq. (1) can be rewritten as the sum of the Fourier time series as a function of time and depth (Andújar M´arquez, et al., 2016; Assouline et al., 2019).

$$T(x,t) = T_{o,t} + \sum_{n=1}^{\infty} T_n \exp\left\{-x\sqrt{\frac{n\pi}{\alpha t_n}}\right\} \sin\left(\frac{2n\pi}{t_o}t + x\sqrt{\frac{n\pi}{\alpha t_n}} + \vartheta_n\right) \tag{2}$$

where $T(x,t)$ is the temperature at burial depth x and time t; $T_{0,t}$: annual mean temperature at x=0; T_n: amplitude of temperature for the nth period; $\alpha = \lambda/\rho C_p$, thermal diffusivity (m^2/s); and ϑ_n: phase shift of temperature in the n^{th} period.

During winter with snow cover, we assume that solar radiation and climate forcing are blocked effectively by the snow in a short period of time window during early winter, and subsurface temperature variation near ground surface is governed by a single constant upward heat flow from the Earth. Under this condition, we can treat the upward heat flow as a steady-state heat flow, while the temperature difference from 0.0 °C (due to latent effect at the contact between snow cover and ground surface) at a given depth from ground surface can be approximated by the Fourier's law:

$$\Delta T = \frac{q}{\lambda}\Delta Z \tag{3}$$

where q is the heat flow (W/m^2), Δz (m) distance downward from ground surface, and ΔT: temperature increase from 0.0 °C.

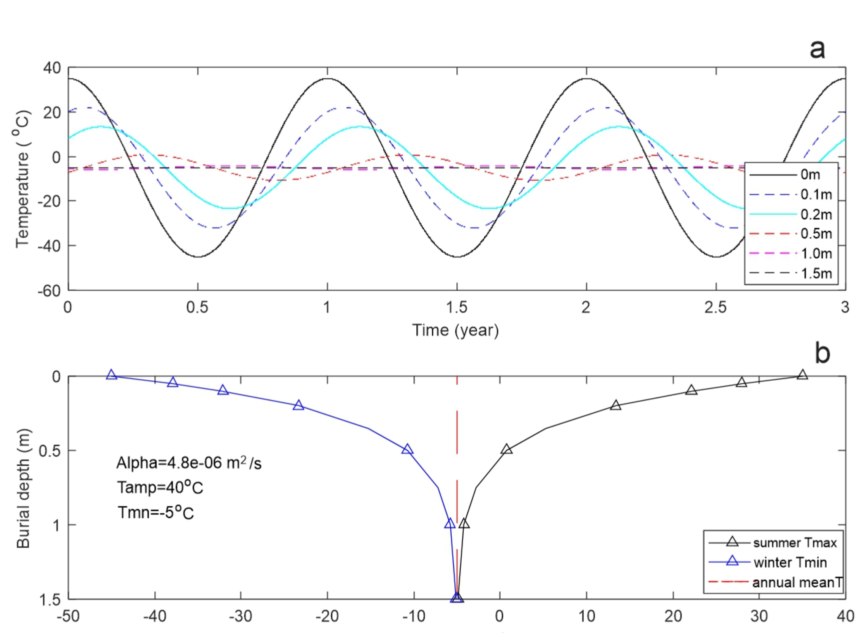

Fig. 3. Diagram showing annual temperature cycles with seasonal fluctuations at and near ground surface as a function of burial depth and responding to surface and subsurface heat fluxes. a) the magnitudes of the temperature decreases with burial depth and a phase shift in time domain. b) the temperature variation as a function of burial depth and surface temperature: on the left winter minimum, and on the right summer maximum, showing the impacts of surface down heat flux on the near-surface temperature variation. For example, at depth 0.5m, the annual minimum and maximum are -10.71 and -0.71 °C, respectively, with ±5.71 °C deviation from annual air temperature mean of 5 °C with maximum and minimum of 35 and -45 °C respectively.

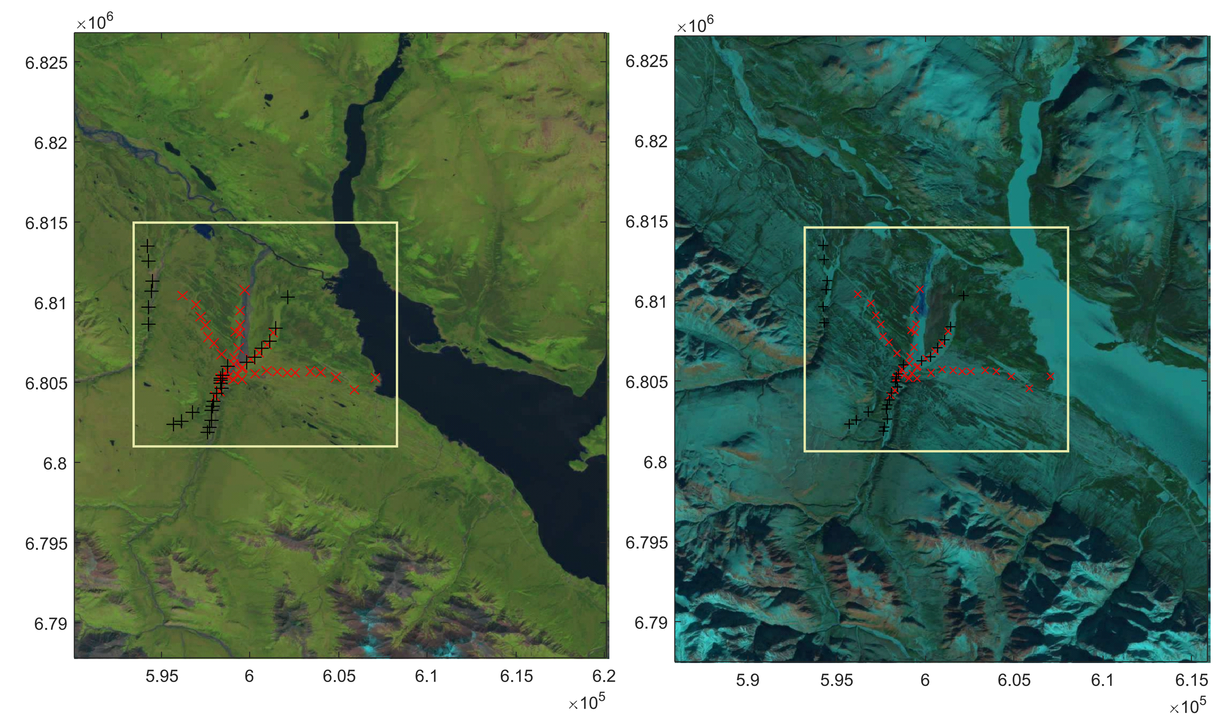

Figure 2. Landsat-8 true colour (BGR) images acquired from different times: Left: summer season (2014-07-22) for features associated with vegetation, water, soil and other land-surface properties; Right: Winter season (2014-02-17) for land surface temperature anomalies. The Yellow squires indicate the area of GST monitoring network, and red cross (GSC) and black cross (YGS) location of GST stations.

Ground Surface Temperature Monitoring Data

The ground surface temperature (GST) data were collected using temperature data loggers (HOBO Water Temp Pro v2) that were deployed in 2022 field season. A total of 65 stations were set in the study area that recorded GST from July 2022 to September 2023 with a programed temperature record for every 30 minutes. Two temperature logger were deployed at each station, one at near ground surface with burial depth of 10 – 20 cm, and a deeper logger in depth range from 40 to 70 cm depending on soil condition at the station (Fig. 4). Two temperature loggers (at GSC stations #4 and 14) were set >1 m above the ground and under shade to record the air temperature as reference air temperature. For details of data collection and surface and topographic conditions, and quantitative measure for the impacts of vegetation on GST records, readers are referred to Chen et al. (2023). Table 1 summarizes the essential environmental variables and in-situ measured soil properties at each monitoring station.

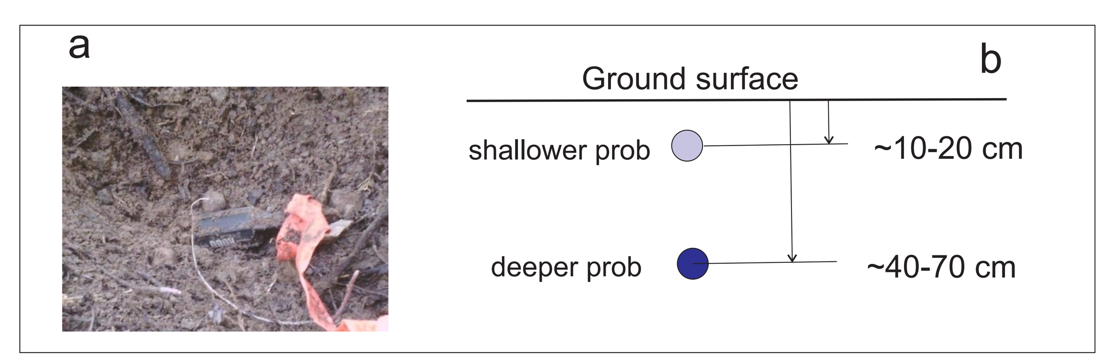

Fig. 4 a): a retrieved HOBO Pro v2 temperature prob from monitoring site; b) configuration of a dual prob deployment at each station.

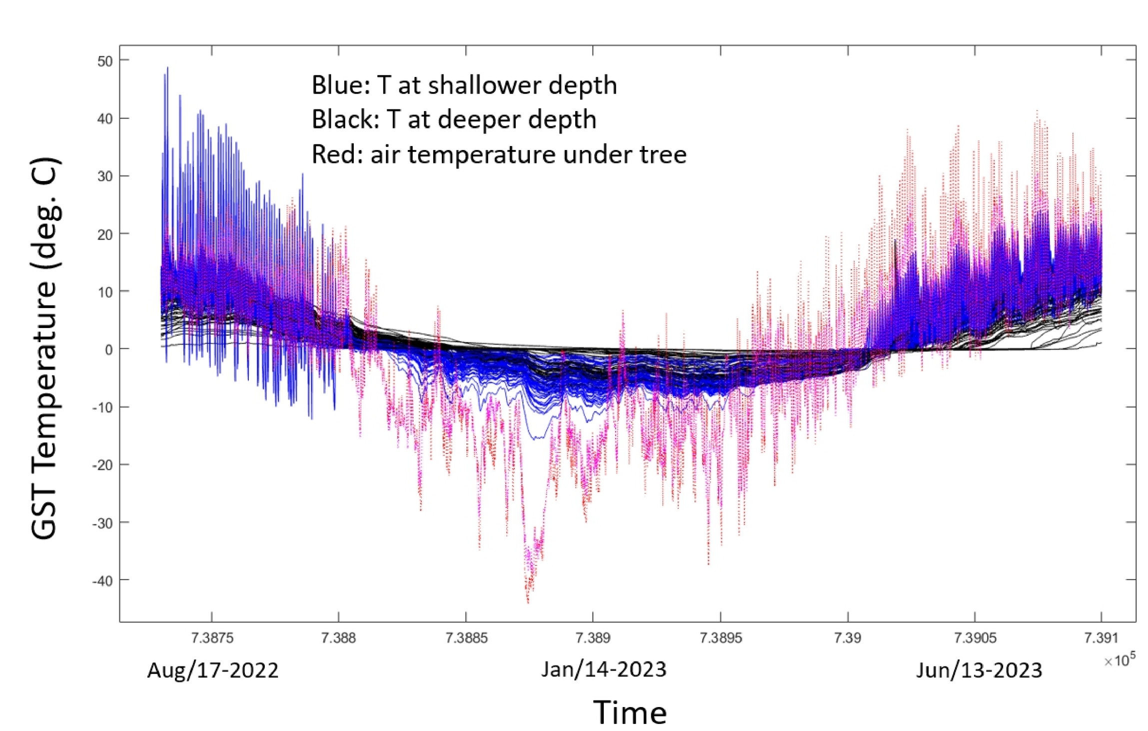

Figure 5. GST time series from the 65 retrieved temperature loggers showing daily temperature cycles, seasonal variation and annual cycle. Although the air temperature plugged below °C in winter, several temperature loggers at deeper position show temperature at around zero during almost entire winter, differing from the others with similar burial depth.

ABSTRACT

Finding renewable energy resources to meet government goals of achieving net-zero emissions by 2050 is one of the greatest challenges we are facing, particularly in the north. Northern communities are largely disconnected from the North American energy grid and rely instead on imported hydrocarbons for heat and electricity. Previous study (e.g Grasby et al., 2011) suggested that Yukon and NE BC as high potential regions for geothermal resources. Additional work shows the potential for geothermal energy to support northern communities (Grasby et al., 2012). Novel geophysical and remote sensing and ground surface temperature (GST) monitoring techniques for geothermal assessment have been developed as part of the Garibaldi geothermal project (Grasby et al., 2021; Chen et al. 2023). This study explore the feasibility of using remotely sensed multi-spectral images from Landsat 8 and GST time series from GST monitoring network to reveal the relationship between deep fault system and subsurface heat flow as a geothermal resource evaluation tool for Canada north. GSC and YSG have deployed a ground surface temperature monitoring network in the summer of 2022, and data from 65 stations were retrieved in the 2023 field season. Preliminary processing was performed to detect areas of elevated heat flow. Two sets of Landsat-8 multispectral images in the Burwash Landing area from different seasons have been collected and processed for feature extraction using ML algorithms. The GST data and features extracted from Landsat images were analysed to ascertain if the geothermal anomalies are related to specific geological features, such as deep fault systems. Here we report the preliminary results with emphasis on GST data analysis.

Table 1. Summary table of the location of GST stations and other parameters for the temperature logger deployment and in-situ measured environment parameters of the soils.

Station #	Latitude	Longitude	Bottom T (°C)	moisture (%)	Thermal conductivity (W/K/m)	Thermal emisivity	Depth A (cm)	Depth B (cm)	Data file	Notes
1	61.3675	-139.0386111	7.7	50	1.251	1.179	70	20	1.csv	GSC
2	61.37138889	-139.0652778	6.8	19.9	0.221	3.714	50	15	2.csv	GSC
3	61.37083333	-139.0897222	7.8	19.6	0.587	NA	40	10	3.csv	GSC
4	61.37222222	-139.1113889	4.9	21.9	0.249	0.159	45	15	4.csv	GSC
5	61.37388889	-139.1377778	10.3	20	0.388	NA	50	20	5.csv	GSC
6	61.38	-139.145	8.5	21	0.741	NA	50	20	6.csv	GSC
7	61.39361111	-139.1383333	8.5	23.5	0.401	NA	50	20	7.csv	GSC
9	61.41777778	-139.1319444	9.7	50	1.549	0.954	60	20	9.csv	GSC
10	61.38833333	-139.1658333	2.7	35.5	0.282	0.178	45	10	10.csv	GSC
11	61.39861111	-139.1744444	8.5	36.2	1.055	NA	50	10	11.csv	GSC
12	61.41027778	-139.1836111	5.7	21.3	0.237	0.954	45	10	12.csv	GSC
13	61.37	-139.1569444	6.9	30.5	0.3	0.258	65	10	13.csv	GSC
14	61.37277778	-139.1530556	5.9	50	0.4	0.621	55	15	14.csv	GSC
15	61.37027778	-139.1427778	5.6	35.5	0.186	1.781	40	10	15.csv	GSC
16	61.36944444	-139.1519444	8	22.4	0.399	NA	40	10	16.csv	GSC
17	61.36027778	-139.0194444	7.5	46.2	0.841	0.446	60	15	17.csv	GSC
18	61.37055556	-139.0544444	7.6	23	0.002	0	40	10	18.csv	GSC
19	61.37055556	-139.0811111	7.7	25.5	0.662	NA	40	10	19.csv	GSC
20	61.37166667	-139.1	9.5	17.6	0.005	0	40	10	20.csv	GSC
21	61.37055556	-139.1233333	4.9	21.5	0.514	0.831	40	10	21.csv	GSC
22	61.37444444	-139.1363889	10	16.5	0.114	0.442	40	10	22.csv	GSC
23	61.37888889	-139.1277778	10	21.2	0.587	NA	40	10	23.csv	GSC
24	61.3825	-139.1183333	8.1	34.2	0.405	NA	45	10	24.csv	GSC
25	61.38694444	-139.11	8.5	21	0.675	NA	40	10	25.csv	GSC
26	61.39333333	-139.1030556	7.5	25.6	0.257	NA	50	10	26.csv	GSC
27	61.41555556	-139.1977778	5.7	24.6	0.313	0.284	50	10	27.csv	GSC
28	61.40333333	-139.1794444	5.4	33.5	0.466	0.296	50	10	28.csv	GSC
29	61.39194444	-139.1719444	4.6	25	0.489	0.255	60	10	29.csv	GSC
30	61.38222222	-139.1583333	3.6	35	0.723	0.352	40	10	30.csv	GSC
31	61.36666667	-138.9972222	7.9	23.5	0.492	NA	45	10	31.csv	GSC
32	61.37638889	-139.1461111	4.8	23.8			40	10	32.csv	GSC
33	61.39805556	-139.1375	8.5	23.8	0.193	0.118	50	10	33.csv	GSC
34	61.39444444	-139.1426111	6.5	28.01	0.597	NA	40	10	34.csv	GSC
37	61.36777778	-139.1466667	6.1	28.1	0.542	0.786	45	10	37.csv	GSC
38	61.36777778	-139.1377778	6.8	20.7	0.627	2.91	45	10	38.csv	GSC
39	61.35861111	-139.1663889	6.1	50	1.653	1.752	55	10	39.csv	GSC
40	61.36138889	-139.1616667	7.3	28.7	0.847	1.718	60	10	40.csv	GSC
41	61.36805556	-139.1602778	4.8	50	0.963	0.618	42	10	41.csv	GSC
YGS_1	61.418425	-139.230464	8.3	31	0.539	NA	51	11	YGS1.csv	YGS
YGS_2	61.409261	-139.234276	8.2	28.8	0.576	1.05	50	11	YGS2.csv	YGS
YGS_3	61.37734	-139.13254	8.4	28.54	0.843	NA	46	10	YGS3.csv	YGS
YGS_4	61.35076	-139.17059	7.2	37.7	1.22	0.645	48	10	YGS4.csv	YGS
YGS_8	61.35589	-139.16806	7.1	32	0.415	0.133	50	12	YGS8.csv	YGS
YGS_9	61.423795	-139.229279	7.9	30.7	0.167	NA	47	10	YGS9.csv	YGS
YGS_10	61.395975	-139.100383	7.3	32.1	0.465	NA	46	12	YGS10.csv	YGS
YGS_11	61.388869	-139.107037	6.5	31.9	17:45	NA	38	10	YGS11.csv	YGS
YGS_12	61.375488	-139.152015	7.8	42.1	0.04	0.083	48	12	YGS12.csv	YGS
YGS_16	61.41325	-139.08607	5.6	27.2	0.435	NA	47	10	YGS16.csv	YGS
YGS_17	61.40796	-139.09673	6.5	20.5	0.372	NA	48	10	YGS17.csv	YGS
YGS_18	61.40178	-139.10049	7	26.2	0.255	NA	39	10	YGS18.csv	YGS
YGS_19	61.37973	-139.12309	7.2	23.1	3.032	NA	48	11	YGS19.csv	YGS
YGS_20	61.38467	-139.11562	7.4	21.1	0.335	NA	44	10	YGS20.csv	YGS
YGS_21	61.399874	-139.234154	8.5	27	0.852	NA	48	12	YGS21.csv	YGS
YGS_22	61.443507	-139.23273	8.5	21.5	0.574	1.586	45	11	YGS22.csv	YGS
YGS_24	61.435281	-139.232077	8.4	27.5	0.326	NA	51	11	YGS24.csv	YGS
YGS_25	61.36017	-139.16484	7.4	50	1.922	1.147	50	10	YGS25.csv	YGS
YGS_26	61.36303	-139.15901	7.3	50	0.606	2.091	56	13	YGS26.csv	YGS
YGS_27	61.36589	-139.1604	6.8	50	0.691	0.358	46	11	YGS27.csv	YGS
YGS_28	61.37019	-139.15753	7.3	25.2	0.502	2.854	56	12	YGS28.csv	YGS
YGS_29	61.345299	-139.170735	5.4	22.8	0.678	NA	48	14	YGS29.csv	YGS
YGS_33	61.36887	-139.15967	6.3	35.5	0.592	2.895	55	10	YGS33.csv	YGS
YGS_34	61.36741	-139.16003	5.1	50	0.14	0.298	48	12	YGS34.csv	YGS

REFERENCES

Chen, Z., Grasby, S., Yuan, W. and Liu X., 2022. Ground surface temperature monitoring data analysis and applications to geothermal exploration in volcanic areas, Mount Meager, western Canada, Geothermics, 108 (2023) 102610, http://creativecommons.org/licenses/by-nc-nd/4.0/
Grasby SE, Allen DM, Bell S, Chen Z, Ferguson G, Jessop A, Kelman M, Ko M, Majorowicz J, Moore M, Raymond J and Therrien R, 2012. Geothermal energy resource potential of Canada, Geological Survey of Canada, Open File 6914.
Grasby, S.E., Ansari, S.M., Calahorrano-Di Patre, A., Chen, Z., Craven, J.A., Dettmer, J., Gilbert, H., Hanneson, C., Harris, M., Liu, J., Muhammad, M., Russell, K., Salvage, R. O., Savard, G., Tschirhart, V., Unsworth, M.J., Vigouroux-Caillibot, N. and Williams- Jones, G. (2021): Geothermal resource potential of the Garibaldi volcanic belt, southwestern British Columbia (part of NTS 092 J); in Geoscience BC Summary of Activities 2020: Energy and Water, Geoscience BC, Report 2021-02, p. 119–122.
Yukon Geological Survey, 2023. A Digital Atlas of Terranes for the Northern Cordillera: Yukon Geological Survey. 2023. Available online: https://data.geology.gov.yk.ca/Compilation/2 (accessed on Nov. 1, 2023).

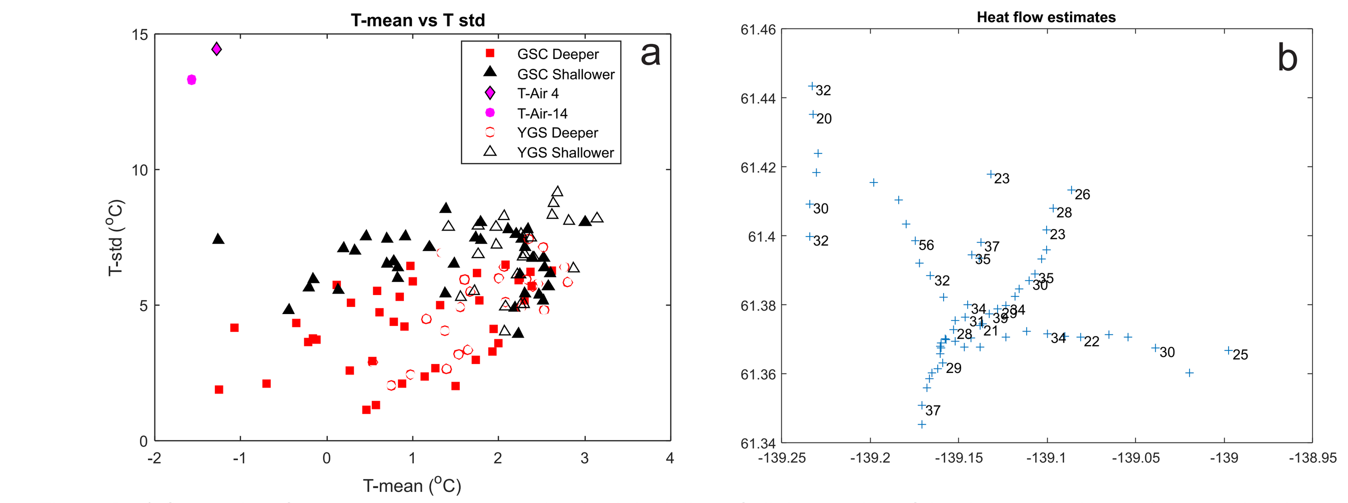

Figure 6. a) Cross plot of temperature mean vs. standard deviation of all time series of the data set in the study area, showing a positive correlation between the two. This means that higher average temperature is likely accompanied by a higher standard deviation. As a reference, the mean and standard deviations from air temperature are also plotted in the graph. Stations with high mean and standard deviation are usually associated with station with less vegetation or shade. b) Map view of the uncorrected heat flow estimates from retrieved GST data (Eq. 3). The thermal conductivities are from the in-situ measurements. Study (Chen et al. 2023) suggested that environmental factors, such as vegetation, soil moisture, elevation and shadiness, have significant impacts on the GST. There are no corrections made to the recorded temperatures at all sites prior to the heat flow estimation. The other factor that affect the heat flow estimation is the latent effect. Data logger near water table or close to permafrost could be affected. The winter snow may not provide sufficient insulation to allow a steady state in temperature for accurate estimation for heat flow directly from raw data.

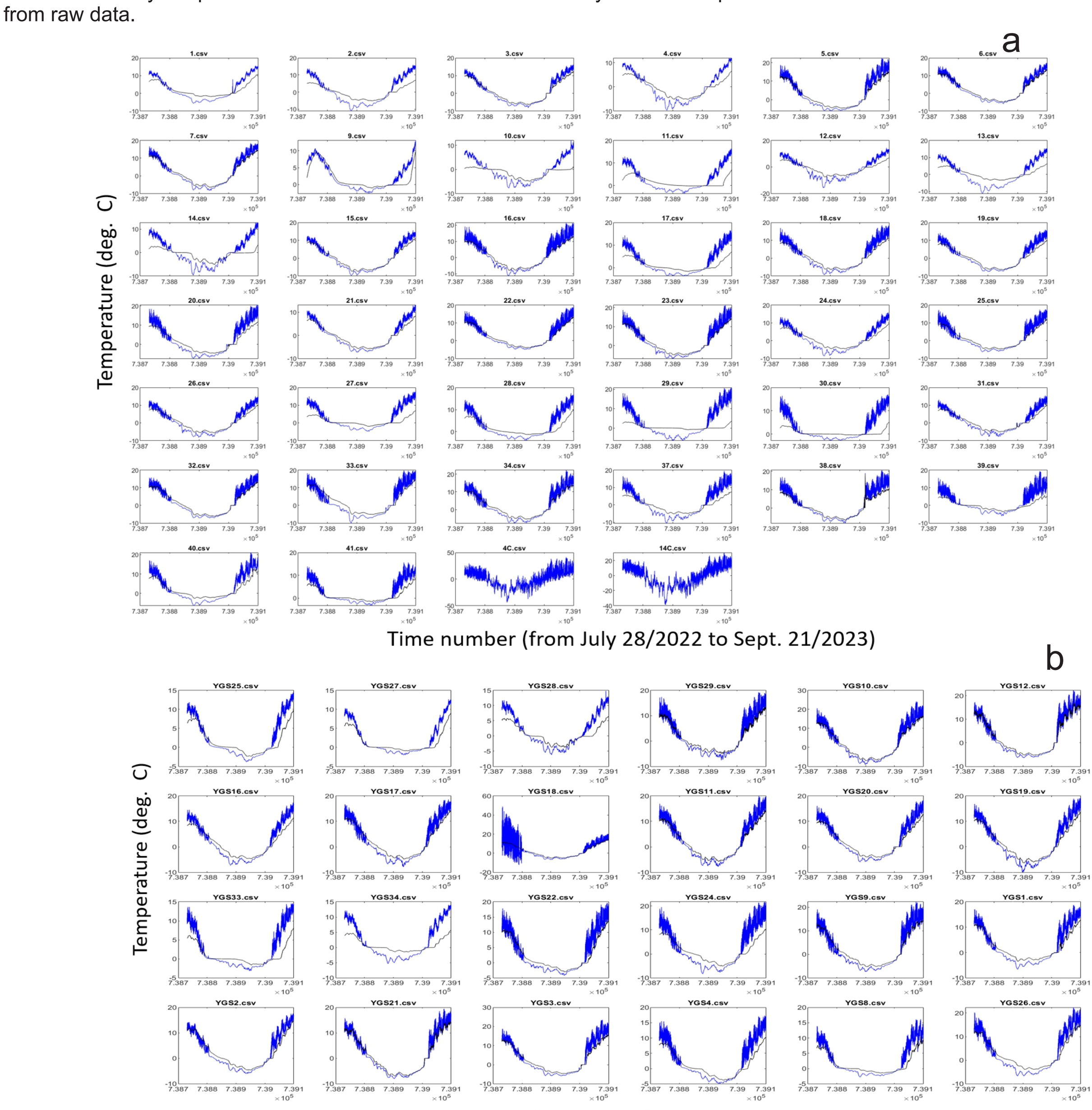

Figure 7. a) Recorded 76 ground surface temperature time series and 2 air temperature time series from 38 monitoring stations employed by GSC, b) 48 GST time series from 24 stations deployed by YGS. For the GST curves, the blue one is from the shallow temperature logger and black one the deeper logger. The shallow GST curve shows clear daily temperature cycles during the summer season, but the daily variations are depressed in winter when snow cover blocked partly the weather forcing. The GST deeper curve receives less solar energy and mild cold weather forcing, and shows no daily cycle in general. The YGS 18 shallow temperature curve shows an unusual daily fluctuations in the first non-snow season because the daily variation is greater than air temperature (Figure 5). It is therefore, inferred that shallower logger was exposed directly under the sun strike. However, in the second non-snow season, it returned to normal (covered by leaves?). The GST curves from the deeper logger show two general styles, the V-shaped curve having a similar annual variation as the shallow curve (e.g., 3, 15 and 16 and YGS10 and 20). The U-shaped curve turns to flat around zero for the entire winter season (9, 20, 30, and YGS8 and 34), suggesting some thermal buffering effects

SUMMARY

The GST data were retrieved in the late September 2023 and the GST monitoring network was deployed in July, 2022 summer field season. The poster presents the raw data and results of preliminary data analysis and parameter estimation without environmental corrections. Uncorrected data suggest spatial patterns for the high average winter temperature data points and high heat flow estimates. The relation between GST and LST remains to be interpreted. It seams that GST records from the monitoring network provide useful insights for better understand the heat flow and its spatial variation. However, direct observations of deep soil properties, permafrost distribution, as well as heat flow estimates from geothermal wells could help calibrate and interpret the GST data and integrate with other data.

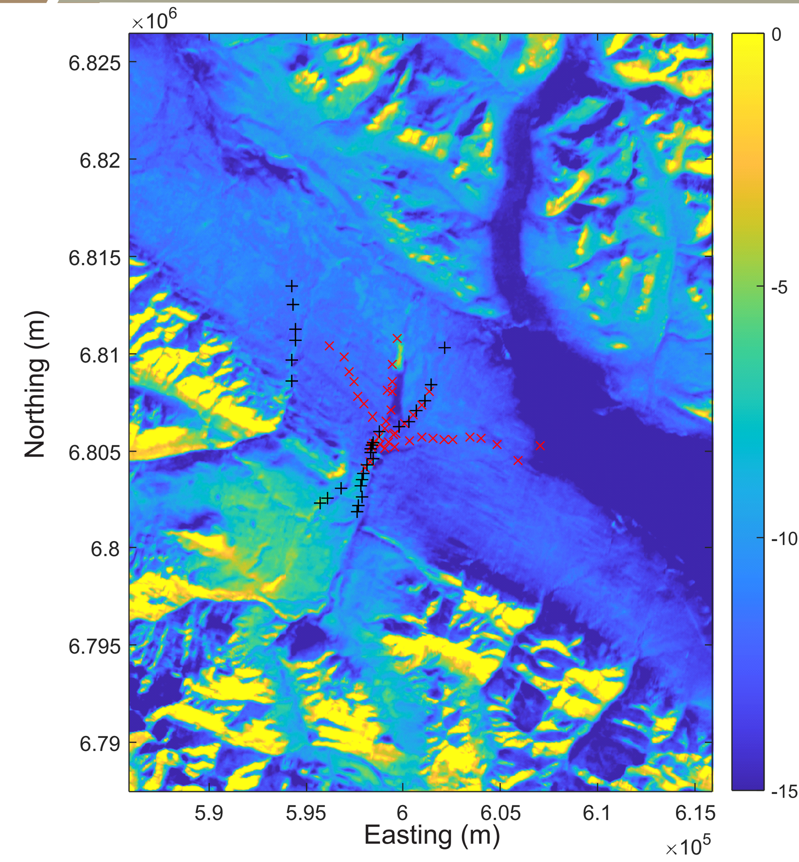

Figure 8. Map view of estimated land surface temperature (LST) from Landsat-8 (2014-02-17) at around 10 am in 2014 winter. The crosses are the GST sites of (red: GSC and black YGS) from July, 2022 - September 2023.

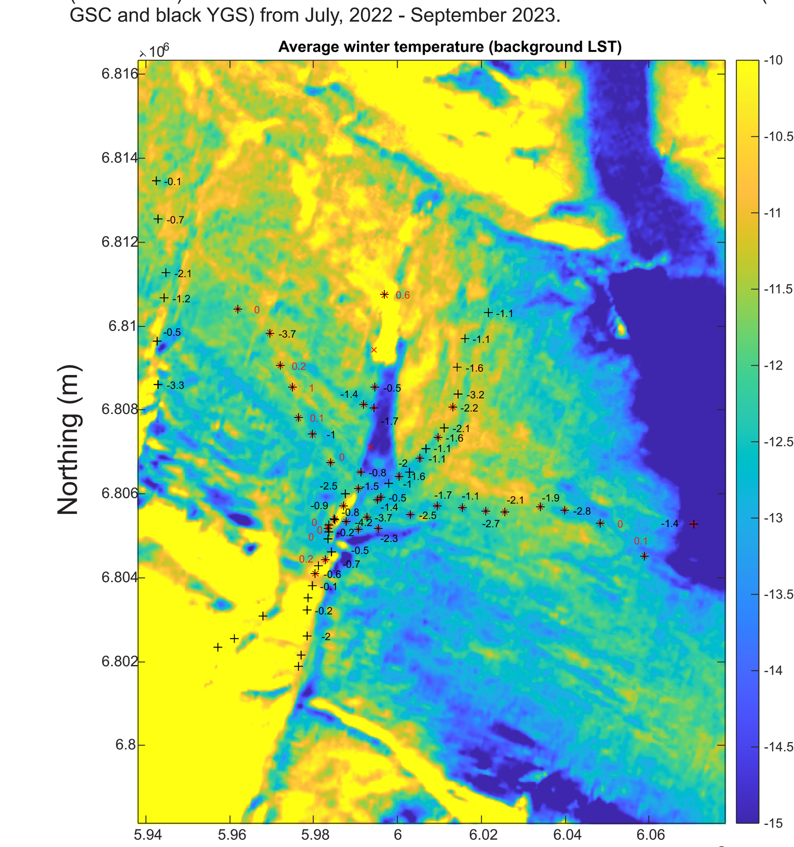

Figure 9. Map view showing the average winter temperature on the background of Land Surface Temperature from Landsat images. High temperature sites are colour coded (RED). It is interesting to know that the high average winter temperature sites are concentrated in west-ceneral part of the study area. Please know that there is no environmental fact corrections mode on the recorded GST temperature.

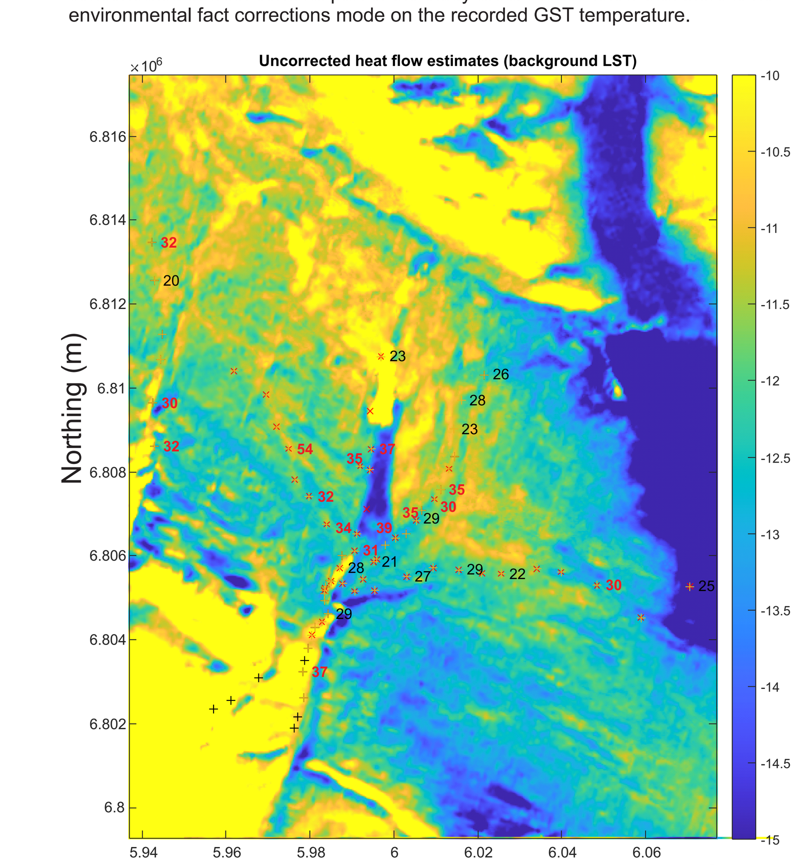

Figure 10 Map view showing the uncorrected heat flow estimates on the background of Land Surface Temperature from Landsat images. High heat flow sites are also concentrated in western-central part, and may or may be coincident with high Land Surface temperature on the map. The sites with heat flow>30 are marked by red. The aligned high LST strips in NNE-SSW in the river valley may represent some subsurface geological features that requires further study.

[1]Natural Resources Canada, Geological Survey of Canada, 3303-33rd Street N.W., Calgary, Alberta T2L 2A7
[2]Yukon Geological Survey, 91807 Alaska Highway, Whitehorse, Yukon Y1A 0R3

For more information, please contact W. Yuan (wanju.yuan@nrcan-rncan.gc.ca).

Permanent link: https://doi.org/10.4095/p15d0hqc2g

This publication is available for free download through the NRCan Open Science and Technology Repository (https://ostrnrcan-dostrncan.canada.ca).

OPEN FILE
DOSSIER PUBLIC
9177
GEOLOGICAL SURVEY OF CANADA
COMMISSION GÉOLOGIQUE DU CANADA
2024

Publications in this series have not been edited; they are released as submitted by the author.

Les publications de cette série ne sont pas révisées; elles sont publiées telles que soumises par l'auteur.

ISSN 2816-7155
ISBN 978-0-660-71355-7
Catalogue No. M183-2/9177E-PDF
https://doi.org/10.4095/p15d0hqc2g

Recommended citation
Chen , Z., Grasby, S.E., Yuan, W. , Colpron, M., and Liu, X., 2024. Methodology study of geothermal resource evaluation using remote-sensing and ground-surface temperature data, Burwash Landing, Yukon – status and preliminary results; Geological Survey of Canada, Open File 9177, 1 poster. https://doi.org/10.4095/p15d0hqc2g